Hindawi
Advances in Condensed Matter Physics
Volume 2018, Article ID 3507176, 8 pages
https://doi.org/10.1155/2018/3507176

Research Article

Total Internal Reflection in a Hybrid Nematic Cell Submitted to Weak Boundary Conditions

Carlos I. Mendoza[1] **and Juan Adrian Reyes**[2]

[1]*Instituto de Investigaciones en Materiales, Universidad Nacional Autónoma de México, Apdo. Postal 70-360, 04510 Ciudad de México, Mexico*
[2]*Instituto de Física, Universidad Nacional Autónoma de México, Apdo. Postal 20-364, 01000 Ciudad de México, Mexico*

Correspondence should be addressed to Juan Adrian Reyes; adrian@fisica.unam.mx

Received 11 December 2017; Revised 3 February 2018; Accepted 26 February 2018; Published 12 April 2018

Academic Editor: Luis L. Bonilla

We calculate the trajectory of a monochromatic optical beam propagating in a planar-homeotropic hybrid nematic crystal cell submitted to weak anchoring conditions. We apply a uniform electric field perpendicular to the cell to control the trajectories for various values of the anchoring elastic energy. We have found that the anchoring energy has a strong influence on the ray penetration length and trajectory. Our calculations are consistent with a previously found Frederick's type transition only present for weak anchoring in which electric fields above an anchoring-energy dependent critical field align completely the director field.

1. Introduction

The total internal reflection in hybrid nematic cell has been studied a time ago in a series of papers [1–3]. The authors report theory and experiments for an optical method based on observing the interference fringes of a beam reflected by a nematic cell that are used to know the local orientation of the molecular director inside the cell. Furthermore, they show that using this method it is possible to get information about the nematic anchoring conditions. In the present report we consider an analogous system but we use a different theoretical approach. Based on geometrical optics arguments, we derive the ray trajectories inside the cell since we are interested in using the total internal reflection as a mechanism for beam steering in optical devices.

Electrooptical devices such as lenses with variable focal distance, dynamic diffraction gratings, and tunable prisms are extremely useful in many applications, for instance, those concerning telecommunication, machine vision, displays, data storage, measurement equipment, and so on. Diffractive optical elements have many advantages over refractive elements [4, 5]; they can rapidly steer, stabilize, and increase reality by reducing costs. They are also small enough to be portable and can be adapted for micron-scaled optical systems. A nematic liquid crystal has a molecular architecture which makes it a medium with a direction-dependent refractive index [5]. By imposing an external electric field to the liquid crystal, it induces variations in the refractive index distribution and in the phase of light waves traveling through it which produces a modification on the direction of propagation of light through the medium. Liquid crystal devices can be much smaller and have less weight than conventional glass and plastic analogues. In addition, they can be integrated into other optical components and compact systems [5]. Different types of optical elements based on liquid crystals technology have been implemented [4–20]. In particular, liquid crystal technology has been applied to construct diffraction gratings that can electrically modulate the diffraction efficiency [21]. It has been shown [22] that, for a monochromatic beam that enters obliquely onto a nematic hybrid cell, the optical path of the beam can be several times larger than the cell's thickness. Therefore, it is possible to use it as a dispersive media similar to a glass prism. As explained in [22], this device has the advantage that all the emerging beams of different wavelength will emerge parallel to each other although the emerging position is different. In other words, rays of different wavelength travel different distances but the emerging angles are equal due

to ray's momentum conservation. In the cited work [22], hard anchoring conditions for the nematic on the cell plates has been assumed; this means that the orientation of the molecules at the plates is not affected by the applied electric field. This assumption is valid only when the external field energy is weaker than the surface anchoring energy.

An anchoring energy is necessary to describe arbitrary anchoring conditions between the liquid crystal and the solid plates [23] which can be interpreted as an anisotropic part of the interface energy. The anchoring energy and its influence on the configuration provide important information of the liquid crystal surface physics. The physical reasons for the anchoring phenomenon and its microscopic mechanisms have been subject of interest [24]. Some years ago, Yang et al. [25] proposed that the interface energy should be understood as the total sum of energy potentials between the molecules of a liquid crystal and the substrate surface. They have found an expression for the anchoring energy, which has two terms, the first term is the same as the Rapini-Papoular expression; the second is related to the normal of the interface and results from the biaxial property of a NLC induced by the interface. However, the anchoring energy may originate from other physical reasons, such as adsorptive ions [26–30]. General expressions for the nematic configuration considering all these phenomena have been recently obtained for a nematic slab under arbitrary boundary conditions [31]. In [22] strong anchoring conditions were considered; however, experimentally there is a wide range of values for this energy [32, 33], ranging from 10^{-6} J/m^2 to 10^{-3} J/m^2. For this reason, it is important to explore what could be the implications of using weak anchoring energies.

In this work, we calculate the orientational state of a liquid crystal submitted to weak anchoring conditions and to the action of a low frequency electric field. Then, we analyze the effect of changing the surface anchoring energy on the penetration length, the path, and the range of a beam traveling inside a liquid crystal cell and exhibit its notorious influence. This element can be used as the base for a beam steering or a multiplexor device.

2. Equilibrium Configuration

The system under study consists of a pure thermotropic nematic confined between two parallel substrates with refraction indexes N_t and N_b, respectively, as depicted in Figure 1. The cell thickness, l, measured along the z-axis, is small compared to the dimension, L, of the cell plates. The director's initial configuration is spatially homogeneous along the plane x-y and varies with z so that at the boundaries the director

$$\hat{\mathbf{n}} = [\sin\theta(z), 0, \cos\theta(z)], \tag{1}$$

where $\theta(z)$ is the orientational angle defined with respect to the z-axis.

In order to obtain the equilibrium configuration of the director, one has to consider the free energy of the nematic

$$\mathscr{F} = \mathscr{F}_{\text{el}} + \mathscr{F}_{\text{em}} + \mathscr{F}_{h}. \tag{2}$$

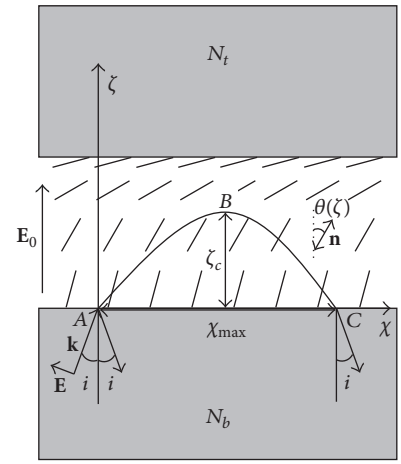

Figure 1: Illustration of a pure thermotropic nematic confined between two parallel substrates. A P-polarized mode is traveling along the hybrid nematic. $N_b, N_t > n_{\parallel}, n_{\perp}$. The trajectory of the beam shows a caustic. ζ_c is the ray penetration. We introduced the dimensionless variables $\zeta \equiv z/l$ and $\chi \equiv x/l$.

The elastic part of the free energy is given by the Frank–Oseen expression [34]

$$\begin{aligned}\mathscr{F}_{\text{el}} = {} & \frac{1}{2}\int_V dV\left[K_1(\nabla\cdot\hat{\mathbf{n}})^2 + K_2(\hat{\mathbf{n}}\cdot\nabla\times\hat{\mathbf{n}})^2\right. \\ & \left. + K_3(\hat{\mathbf{n}}\times\nabla\times\hat{\mathbf{n}})^2\right] + \frac{1}{2}\int_{S_1} W_0\sin^2(\theta-0)\,dS + \frac{1}{2} \\ & \cdot\int_{S_2} W_0\sin^2\left(\theta-\frac{\pi}{2}\right)dS - \int_V K_{24}\nabla\cdot[\hat{\mathbf{n}}\nabla\cdot\hat{\mathbf{n}} \\ & + \hat{\mathbf{n}}\times\nabla\times\hat{\mathbf{n}}],\end{aligned} \tag{3}$$

where the elastic moduli K_1, K_2, and K_3 correspond to transverse bending splay, twist, and longitudinal bending deformations, respectively. Here K_{24} is the surface elastic constant. The term associated with this constant does not enter the Euler–Lagrange variational derivative for the bulk because it can be transformed in a surface term by using Gauss theorem. However, it can contribute to the energy and influence the equilibrium director through boundary conditions. Nevertheless for this particular planar geometry, this term is null as it is proved in [34].

W_0 is a parameter having units of energy per area and is associated with the interaction between the nematic molecules and the confining surfaces. The first integral involved is on the volume of the LC contained between the planar cell and the second and third ones should be performed over the upper and lower plates and are denoted by S_1 and S_2, respectively.

A low frequency uniform electric field E_0 parallel to the z-axis is applied. Thus, the electric contribution to the energy is

$$\mathscr{F}_{\text{em}} = -\frac{1}{2}\int_V \mathbf{D}\cdot\mathbf{E}\,dV = -\frac{1}{2}\int_V \epsilon_{zz}E^2 dV. \tag{4}$$

Here, $\mathbf{D}$ is the electric displacement vector and ϵ_{zz} is the zz component of the dielectric tensor.

The total free energy of the LC is obtained by expressing the integrals of (3) and (4) in Cartesian coordinates to obtain the free energy per unit length, and introducing the variable $\zeta = z/l$,

$$\mathscr{F} = \int_0^1 d\zeta f_B\left(\theta, \frac{d\theta}{d\zeta}\right) + f_S\left[\theta(0), \theta(l)\right], \tag{5}$$

where

$$f_B\left(\theta, \frac{d\theta}{d\zeta}\right) = \frac{\pi K_1}{2}\left[\left(\frac{d\theta}{d\zeta}\right)^2\left(\sin^2\theta + \kappa\cos^2\theta\right)\right] - \pi K_1 q\left(\cos^2\theta + \frac{\varepsilon_\perp}{\varepsilon_a}\right), \tag{6}$$

where $\kappa = K_3/K_1$, $q \equiv \varepsilon_a E^2/(2K_1)$, and $\varepsilon_\perp$ and $\varepsilon_\parallel$ are the low frequency dielectric constants perpendicular and parallel to the director and $\varepsilon_a \equiv \varepsilon_\parallel - \varepsilon_\perp$ is the dielectric anisotropy.

$$f_S\left[\theta(0), \theta(l)\right] = \pi\left[w_1\sin^2(\theta) + w_2\sin^2\left(\theta - \frac{\pi}{2}\right)\right]. \tag{7}$$

To find the equilibrium condition we need to calculate the variation of the energy $\mathscr{F}$, as shown in [34]

$$\begin{aligned}\delta\mathscr{F} = \int_0^1 d\zeta\Bigg[&\frac{\partial f_B(\theta, d\theta/d\zeta)}{\partial\theta}\delta\theta \\ &+ \frac{\partial f_B(\theta, d\theta/d\zeta)}{\partial(d\theta/d\zeta)}\delta\left(\frac{d\theta}{d\zeta}\right)\Bigg] + \frac{\partial f_S\left[\theta(0), \theta(l)\right]}{\partial\theta(0)}\delta\theta(0) \\ &+ \frac{\partial f_S\left[\theta(0), \theta(l)\right]}{\partial\theta(l)}\delta\theta(l).\end{aligned} \tag{8}$$

Note that f_S is not an explicit function of ζ; however, it is a function of $\theta(l)$ and $\theta(0)$. To proceed, we interchange the order of the variation and derivatives $\delta(d\theta/d\zeta) = (d/d\zeta)(\delta\theta)$ and use the chain rule for partial derivatives,

$$\begin{aligned}\frac{d}{d\zeta}&\left\{\frac{\partial f_B(\theta, d\theta/d\zeta)}{\partial(d\theta/d\zeta)}\delta\theta\right\} \\ &= \frac{d}{d\zeta}\left\{\frac{\partial f_B(\theta, d\theta/d\zeta)}{\partial(d\theta/d\zeta)}\right\}\delta\theta \\ &\quad + \frac{\partial f_B(\theta, d\theta/d\zeta)}{\partial(d\theta/d\zeta)}\frac{d}{d\zeta}(\delta\theta).\end{aligned} \tag{9}$$

After substitution of these results in (8) we obtain

$$\begin{aligned}\delta\mathscr{F} = \int_0^1 d\zeta\Bigg[&\frac{\partial f_B(\theta, d\theta/d\zeta)}{\partial\theta}\delta\theta \\ &+ \frac{d}{d\zeta}\left\{\frac{\partial f_B(\theta, d\theta/d\zeta)}{\partial(d\theta/d\zeta)}\delta\theta\right\} - \frac{d}{dz}\left\{\frac{\partial f_B(\theta, d\theta/d\zeta)}{\partial(d\theta/d\zeta)}\right\} \\ &\cdot\delta\theta\Bigg] + \frac{\partial f_S\left[\theta(0), \theta(l)\right]}{\partial\theta(0)}\delta\theta(l) + \frac{\partial f_S\left[\theta(0), \theta(l)\right]}{\partial\theta(0)} \\ &\cdot\delta\theta(0).\end{aligned} \tag{10}$$

Upon application of the fundamental theorem of calculus we get

$$\begin{aligned}\delta\mathscr{F} = &\int_0^1 d\zeta\left[\frac{\partial f_B(\theta, d\theta/d\zeta)}{\partial\theta} - \frac{d}{d\zeta}\left\{\frac{\partial f_B(\theta, d\theta/d\zeta)}{\partial(d\theta/d\zeta)}\right\}\right]\delta\theta \\ &+ \left[\frac{\partial f_S\left[\theta(0), \theta(l)\right]}{\partial\theta(l)} + \frac{\partial f_B(\theta, d\theta/d\zeta)}{\partial(d\theta/d\zeta)}\right]\Bigg|_{\zeta=l}\delta\theta(l) \\ &+ \left[\frac{\partial f_S\left[\theta(0), \theta(l)\right]}{\partial\theta(0)} - \frac{\partial f_B(\theta, d\theta/d\zeta)}{\partial(d\theta/d\zeta)}\right]\Bigg|_{\zeta=0}\delta\theta(0).\end{aligned} \tag{11}$$

Finally, to obtain the extrema of this functional we impose the condition $\delta\mathscr{F} = 0$ that has to be valid for all

$$\begin{aligned}&\frac{\partial f_B(\theta, d\theta/d\zeta)}{\partial\theta} - \frac{d}{d\zeta}\left\{\frac{\partial f_B(\theta, d\theta/d\zeta)}{\partial(d\theta/d\zeta)}\right\} = 0, \\ &\left(\frac{\partial f_S\left[\theta(0), \theta(l)\right]}{\partial\theta(l)} + \frac{\partial f_B(\theta, d\theta/d\zeta)}{\partial(d\theta/d\zeta)}\right)\Bigg|_{\zeta=1} = 0, \\ &\left(\frac{\partial f_S\left[\theta(0), \theta(l)\right]}{\partial\theta(0)} - \frac{\partial f_B(\theta, d\theta/d\zeta)}{\partial(d\theta/d\zeta)}\right)\Bigg|_{\zeta=0} = 0.\end{aligned} \tag{12}$$

Notice that the first condition stated in last expression is the usual Euler–Lagrange equation valid even for hard anchoring conditions whereas the two remaining expressions are mixed boundary differential equations for the orientation angle to be fulfilled at the frontiers of the region involved.

Substitution of (6) of the bulk energy in the first condition stated in the latter expression gives

$$\frac{d}{d\zeta}\left[\sin^2\theta + \kappa\cos^2\theta\right]\frac{d\theta}{d\zeta} - q\sin 2\theta = 0. \tag{13}$$

After inserting (6) and (7) in the second and third conditions of (12) we obtain the following explicit expressions for the lower plate:

$$\left.\frac{d\theta}{d\zeta}\right|_{\zeta=0} = \left.\frac{\sigma\sin\theta\cos\theta}{\kappa\cos^2\theta + \sin^2\theta}\right|_{\zeta=0}, \tag{14}$$

and for the upper plate

$$\left.\frac{d\theta}{d\zeta}\right|_{z=1} = \left.\frac{\sigma\sin\theta\cos\theta}{\kappa\cos^2\theta + \sin^2\theta}\right|_{\zeta=1}, \tag{15}$$

where $\sigma = lW_0/K_1$.

To obtain the distribution of the nematic orientation we solve (13) subjected to the boundary conditions (14) and (15). We find numerically the solutions for the nematic phase 5CB at 25.1°C, for which $K_1 = 1.2 * 10^{-11}$ N and $K_3 = 1.57 * 10^{-11}$ N. To do this, we use a Runge Kutta algorithm from the low plate $\zeta = 0$ by using as starting values for $\theta(0)$ and $d\theta(0)/d\xi$, those satisfying (14) with $\theta(0)$, a given trial value. Thus, we calculate $\theta(1)$ and $d\theta(1)/d\xi$ at the top plate and check whether these values satisfy (15). If it is not the case we use another trial value for $\theta(0)$ until we reach the correct configuration [35].

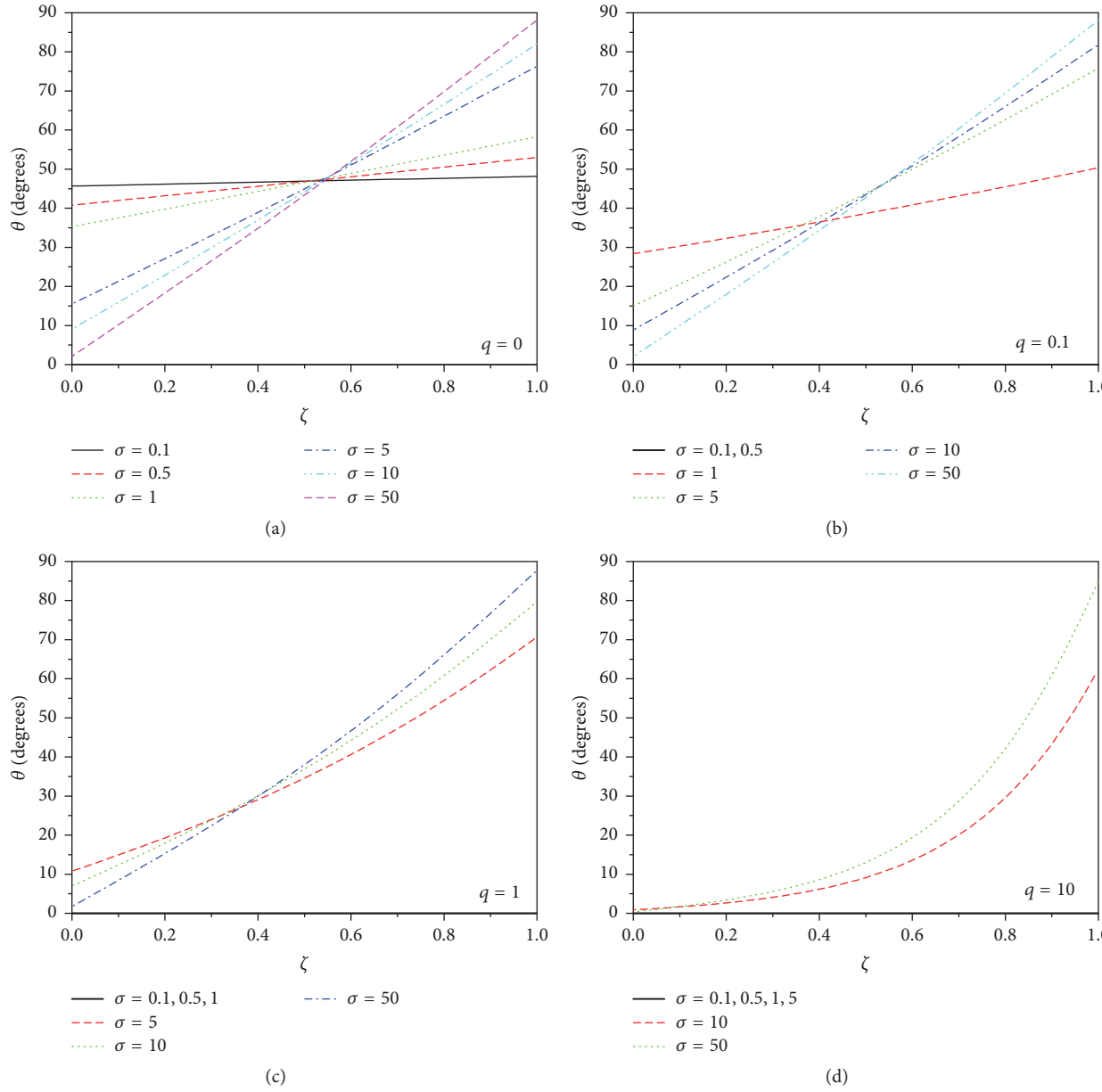

FIGURE 2: Nematic's director as a function of ζ fore 5CB at $T = 25.1^{\circ}$C for (a) $q = 0$, (b) $q = 0.1$, (c) $q = 1$, and (d) $q = 10$.

In Figure 2 we have depicted the orientation versus the dimensionless distance ζ parameterized by the values of σ. The different panels corresponds to various values of the externally applied field q. Figure 2(a) corresponds to $q = 0$ and shows that for the smallest values of σ the nematic orientation is practically uniform. For larger values of σ the spatial dependence keeps almost linear while the slope increases until the configuration converges to the straight line connecting the angles $\theta = 0^{\circ}$ and $\theta = 90^{\circ}$ for the largest value of σ for which we recover hard anchoring conditions. The same trend is observed in Figure 2(b), however, the presence of the field $q = 0.1$ makes that for the smallest values of $\sigma = 0.1$ and 0.5, the molecules of the nematic align completely parallel to the direction of the field, and thus $\theta = 0$ in these cases. Figures 2(c) and 2(d) for $q = 1$ and $q = 10$ exhibit similar trends. Notice that the stronger the field, the larger the number of cases that align perfectly with the field. Note that the curves in Figure 2(d) corresponding to a larger field have a much more pronounced curvature as a consequence of the trend of the molecules to try to align with the field.

In calculating these curves, we have found that when the electric field surpasses certain threshold for a given value of σ, the director aligns completely with the external field and thus conforms a uniform configuration. This result is in agreement with a previously found Frederick's transition obtained by Barbero and colleagues [34, 36]. For completeness we have plotted in Figure 3 this threshold versus the parameter σ. Above this curve, the director is aligned parallel to the field. A more extensive study of this transitional configuration has been done elsewhere [31] under the presence of some other

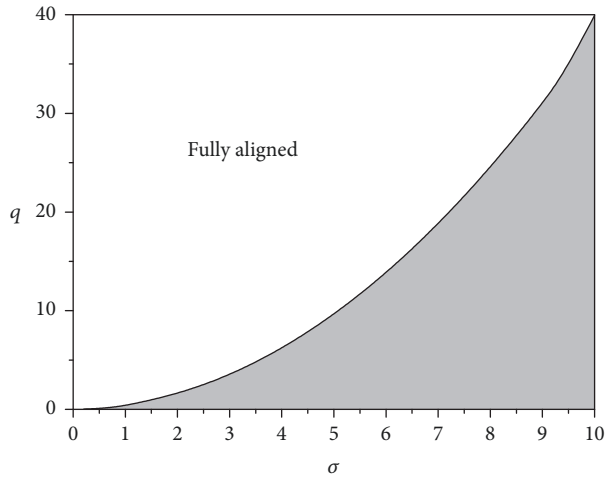

FIGURE 3: Curve that separates the regions where the applied electric field aligns the director in the vertical direction along the whole cell (fully aligned region) and the shaded region where the boundaries still influences the direction of the director which is position dependent as shown in Figure 2.

effects as the presence of adsorptive ions. Indeed, our results are consistent with those found there.

3. Ray Propagation

An obliquely incident light beam with P-polarization (P-wave), that is, with the electric field contained in the incidence plane x-z, impinges the nematic with an incident angle i as shown in Figure 1. The intensity of the beam is low enough so that it does not distort the nematic's configuration. The dynamics of this optical field is described by Maxwell's equations which contain the dielectric tensor ε_{ij}, corresponding to an uniaxial medium which has the general form

$$\varepsilon_{ij} = \varepsilon_{\perp}\delta_{ij} + \varepsilon_a n_i\left[\theta(z)\right] n_j\left[\theta(z)\right], \tag{16}$$

where $\varepsilon_{\perp}$ and $\varepsilon_{\parallel}$ are the dielectric constants perpendicular and parallel to the director and $\varepsilon_a \equiv \varepsilon_{\parallel} - \varepsilon_{\perp}$ is the dielectric anisotropy.

The usual method to solve Maxwell's equations has been carried out in detail for a hybrid cell similar to the one considered here [37], and it is found that there is a regime for the incidence angle i where the ray trajectory presents a caustic, that is, a geometrical place where the beam bends and remains inside the cell until it returns back towards the incidence substrate (see Figure 1). This trajectory is given by [37]

$$\upsilon = \chi - \int_0^{\zeta} d\eta \frac{\varepsilon_{xz} \mp p\sqrt{\varepsilon_{\perp}\varepsilon_{\parallel}}/\sqrt{\varepsilon_{zz} - p^2}}{\varepsilon_{zz}}. \tag{17}$$

In this equation the dimensionless variable $\chi \equiv x/l$ has been introduced, $p \equiv N_b \sin i$ is the ray component in the x direction, and υ is a constant that is determined by the incident point of the beam on the cell; that is, it establishes an initial condition. The $\pm$ sign in (17) corresponds to a ray traveling with $\mathbf{k}$ in the $\pm z$ direction, that is, going from A to B and from B to C, respectively (see Figure 1).

As explained in [38], there are two regimes for i. The first one corresponds to $i - i_c < 0$, with i_c being a critical angle, where all the rays always reach the top substrate and part of the ray is transmitted to the top plate. On the other hand, the second regime corresponds to $i - i_c > 0$, namely, when the beam does not get the top substrate and it is reflected back to the interior of the cell as depicted in Figure 1. Besides i_c, there is a second critical angle, i_{c2}, for which the beam no longer enters the liquid crystal cell and at which it is reflected back to the lower substrate. Here we will consider only angles $i_c < i < i_{c2}$ for which the ray penetrates the cell and is reflected back.

The director's angle at the returning point, θ_c, is given by

$$\theta_c = \arccos\sqrt{\frac{\left(p^2 - \varepsilon_{\perp}\right)}{\varepsilon_a}}, \tag{18}$$

from which the critical angles, i_c and i_{c2}, can be obtained by substituting $\theta_c = \theta(\zeta = 1)$ and $\theta_c = \theta(\zeta = 0)$, respectively. It is worth mentioning that since this formula was derived exclusively from Maxwell's equations, it is independent of the type of anchoring assumed for the orientation at the boundaries.

Figure 4 exhibits the caustic position or penetration length ζ_c as a function of the incidence angle i parameterized with the surface elastic energy parameter σ. Similarly as in Figure 3, the different panels correspond to different field intensities. Figure 4(a) shows that in the absence of field ($q = 0$) the range of incidence angles at which ζ_c goes from zero to one is narrower for smaller values of σ. Figure 4(b) shows that the presence of the field widens the mentioned interval of incidence angles but overcoat for small values of σ. In Figures 4(c) and 4(d) the curves for different values of σ almost merge in one, demonstrating that the surface elastic energy is not playing an important role for large fields.

Figure 5 displays the beam trajectories versus the surface elastic energy parameter where Figures 5(a) and 5(b) correspond to $q = 0$ and $q = 10$, respectively. Figure 5(a) exhibits how the trajectory range changes dramatically on the value of σ when there is no applied field. That is, for the smallest value of σ considered, the beam travels 35 times the thickness of the slab whereas for the largest σ it only travels five times the mentioned thickness. Conversely, Figure 5(b) shows that the trajectory range varies less than one cell thickness on the value of σ when the external electric field is strong. This implies that whether it is needed to design a device for performing a beam steering with large transverse displacements, it is necessary to use a coating for the cell plates which causes a weaker anchoring condition.

4. Conclusions

In this paper we have generalized our previous model for a monochromatic beam impinging obliquely onto a nematic

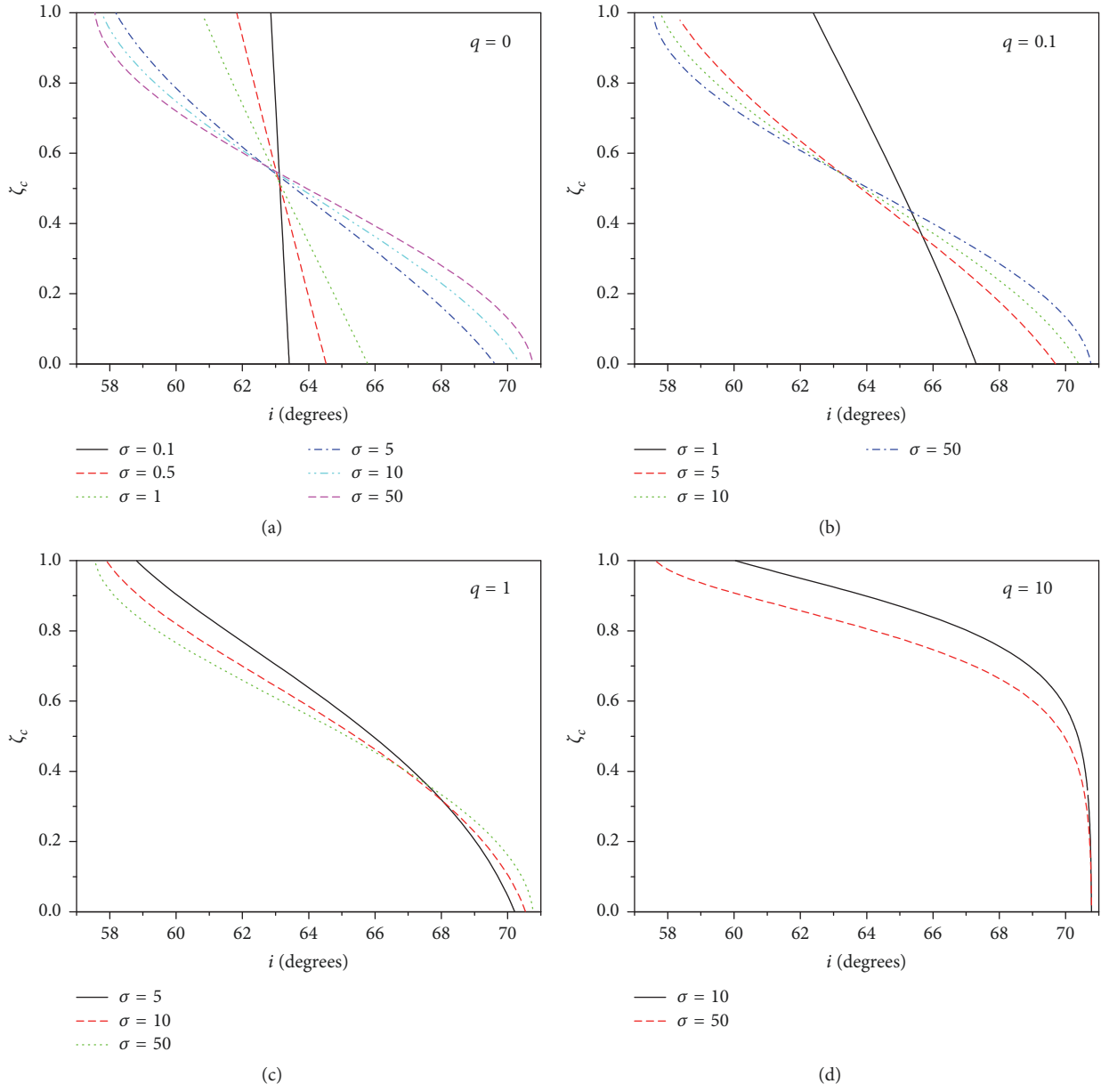

FIGURE 4: Ray penetration ζ_c as function of the angle of incidence for (a) $q = 0$, (b) $q = 0.1$, (c) $q = 1$, and (d) $q = 10$.

hybrid cell, to take into account arbitrary anchoring conditions. We have found that the ray penetration range and trajectory are strongly affected by the anchoring energy. For example, we have shown that under low anchoring surface energies (small σ) the trajectory range could be roughly an order of magnitude larger than those ranges associated with hard anchoring conditions, which already were several times the cell's thickness. Thus, whether an electrooptical instrument is required for performing a beam steering with large transverse range, it would be essential to apply a coating substance with less stickiness at the cell plates in order to weaken the anchoring energy. Since in experiments there is a wide range of values for this energy [32, 33], ranging from 10^{-6} J/m^2 to 10^{-3} J/m^2, our results can be applied to a wide range of systems. Our results consistently confirms previous results [34, 36] for a Fredericks' type transition consisting in a complete alignment of the director field for strong enough applied electric field which is only possible due to the use of weak anchoring. It is worth mentioning that in using this device all the emerging beams whose position can be controlled by the electric field will emerge parallel to each other so this effect is particularly useful for applications requiring to move parallel to a light beam.

Conflicts of Interest

The authors declare that there are no conflicts of interest regarding the publication of this paper. The funds mentioned in Acknowledgments do not lead to any conflicts of interest regarding the publication of this manuscript.

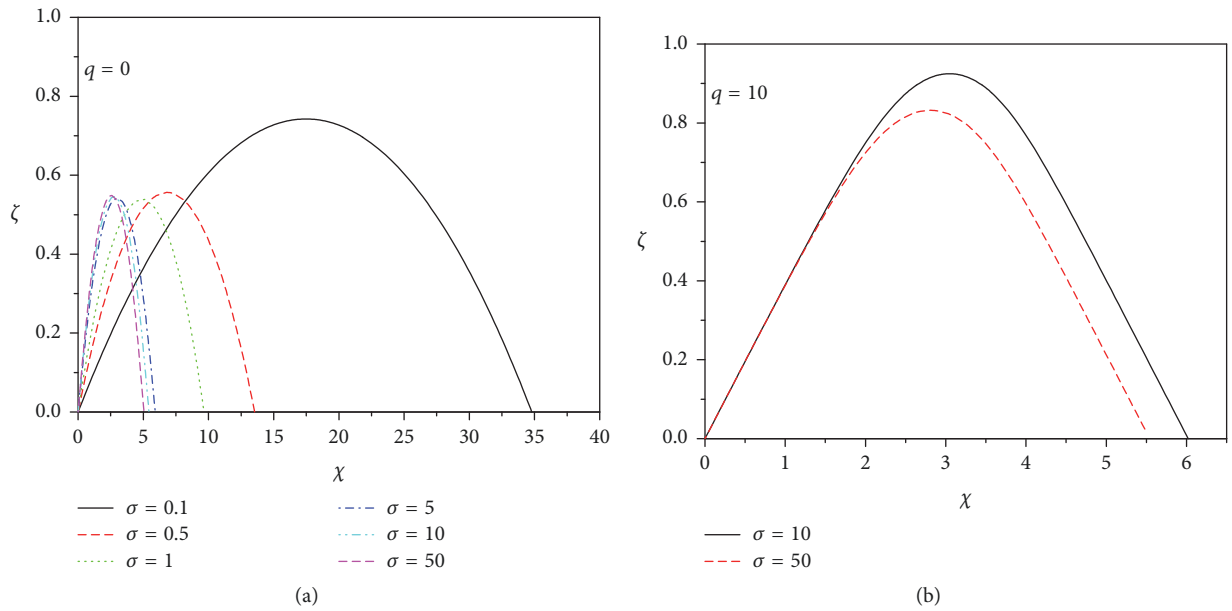

FIGURE 5: Trajectories of the rays for an angle of incidence $i = 63^{\circ}$. Two cases are shown, $q = 0$ and $q = 10$.

Acknowledgments

This work was supported in part by DGAPA-UNAM under Grant nos. IN-110516 (Carlos I. Mendoza) and IN110012.3 (Juan Adrian Reyes).

References

[1] F. Bloisi, L. Vicari, and F. Simoni, "Nonlinear liquid-crystal interfaces: Determination of the local director orientation," *Il Nuovo Cimento D*, vol. 12, no. 9, pp. 1273–1280, 1990.

[2] F. Bloisi, L. R. Vicari, and F. Simoni, "Determination of the Director Orientation Inside a Hybrid Nematic Cell by Total Internal Reflection," *Molecular Crystals and Liquid Crystals Incorporating Nonlinear Optics*, vol. 179, no. 1, pp. 45–55, 2011.

[3] F. Simoni, F. Bloisi, L. Vicari, M. Warenghem, M. Ismaili, and D. Hector, "Optical measurement of local director distribution in a distorted nematic liquid crystal," *EPL (Europhysics Letters)*, vol. 21, no. 2, pp. 189–194, 1993.

[4] P. F. McManamon, P. J. Bos, M. J. Escuti et al., "A review of phased array steering for narrow-band electrooptical systems," *Proceedings of the IEEE*, vol. 97, no. 6, pp. 1078–1096, 2009.

[5] F. Träger, *Springer Handbook of Lasers and Optics*, Springer, 2007.

[6] J. Beeckman, K. Neyts, and P. J. M. Vanbrabant, "Liquid-crystal photonic applications," *Optical Engineering*, vol. 50, no. 8, Article ID 081202, 2011.

[7] A. Akatay, C. Ataman, and H. Urey, "High-resolution beam steering using microlens arrays," *Optics Expresss*, vol. 31, no. 19, pp. 2861–2863, 2006.

[8] T. M. De Jong, D. K. G. De Boer, and C. W. M. Bastiaansen, "Surface-relief and polarization gratings for solar concentrators," *Optics Express*, vol. 19, no. 16, pp. 15127–15142, 2011.

[9] E. Hällstig, T. Martin, L. Sjöqvist, and M. Lindgren, "Polarization properties of a nematic liquid-crystal spatial light modulator for phase modulation," *Journal of the Optical Society of America A: Optics and Image Science, and Vision*, vol. 22, no. 1, pp. 177–184, 2005.

[10] J. Zhang, V. Ostroverkhov, K. D. Singer, V. Reshetnyak, and Y. Reznikov, "Electrically controlled surface diffraction gratings in nematic liquid crystals," *Optics Expresss*, vol. 25, no. 6, pp. 414–416, 2000.

[11] S. Valyukh, I. Valyukh, and V. Chigrinov, "Liquid-crystal based light steering optical elements," *Photonics Letters of Poland*, vol. 3, no. 2, pp. 88–90, 2011.

[12] L. Shi, P. F. McManamon, and P. J. Bos, "Liquid crystal optical phase plate with a variable in-plane gradient," *Journal of Applied Physics*, vol. 104, no. 3, Article ID 033109, 2008.

[13] B. Apter, U. Efron, and E. Bahat-Treidel, "On the fringing-field effect in liquid-crystal beam-steering devices," *Applied Optics*, vol. 43, no. 1, pp. 11–19, 2004.

[14] S. Valyukh and V. Chigrinov, "P-136: Optimization of Liquid-Crystal Phased Arrays," *SID Symposium Digest of Technical Papers*, vol. 42, no. 1, pp. 1619–1622, 2011.

[15] X. Wang, B. Wang, P. J. Bos et al., "Modeling and design of an optimized liquid-crystal optical phased array," *Journal of Applied Physics*, vol. 98, no. 7, Article ID 073101, 2005.

[16] B. Bellini, M. A. Geday, N. Bennis et al., "Design and simulation of single-electrode liquid crystal phased arrays," *Opto-Electronics Review*, vol. 14, no. 4, pp. 269–273, 2006.

[17] J. L. D. Bougrenet and D. L. Tocnaye, "A polymer-dispersed liquid crystal-based dynamic gain equalizer," *Liquid Crystals*, vol. 31, pp. 241–269, 2004.

[18] S. Valyukh, I. Valyukh, V. Chigrinov, H. S. Kwok, and H. Arwin, "Liquid crystal light deflecting devices based on nonuniform anchoring," *Applied Physics Letters*, vol. 97, no. 23, Article ID 231120, 2010.

[19] S. Valyukh, V. Chigrinov, and H. S. Kwok, "A liquid crystal lens with non-uniform anchoring energy," in *Proceedings of the 2008 SID International Symposium*, pp. 659–662, usa, May 2008.

[20] M. Ye, Y. Yokoyama, and S. Sato, "Liquid crystal lens prepared utilizing patterned molecular orientations on cell walls," *Applied Physics Letters*, vol. 89, no. 14, Article ID 141112, 2006.

[21] J. Chen, P. J. Bos, H. Vithana, and D. L. Johnson, "Electro-optically controlled liquid crystal diffraction grating," *Applied Physics Letters*, vol. 67, no. 18, pp. 2588–2590, 1995.

[22] C. I. Mendoza, J. A. Olivares, and J. A. Reyes, "Electrically controlled total internal reflection in nematic hybrid cells," *Physical Review E: Statistical, Nonlinear, and Soft Matter Physics*, vol. 70, no. 6, Article ID 062701, pp. 1–62701, 2004.

[23] A. Sonin, *The Surface Physics of Liquid Crystals*, Gordon and Breach Press, New York, NY, USA, 1995.

[24] B. Jerome, "Surface effects and anchoring in liquid crystals," *Reports on Progress in Physics*, vol. 54, no. 3, article no. 002, pp. 391–451, 1991.

[25] Y. Guo-Chen, Z. Shu-Jing, H. Li-Jun, and G. Rong-Hua, "The formula of anchoring energy for a nematic liquid crystal," *Liquid Crystals*, vol. 31, no. 8, pp. 1093–1100, 2004.

[26] G. Barbero and G. Durand, "Selective ions adsorption and nonlocal anchoring energy in nematic liquid crystals," *Journal of Applied Physics*, vol. 67, no. 5, pp. 2678–2680, 1990.

[27] A. L. Alexe-Ionescu, G. Barbero, and A. G. Petrov, "Gradient flexoelectric effect and thickness dependence of anchoring energy," *Physical Review E: Statistical, Nonlinear, and Soft Matter Physics*, vol. 48, no. 3, pp. R1631–R1634, 1993.

[28] R. Meister and B. Jérôme, "Influence of a surface electric field on the anchoring characteristics of nematic phases at rubbed polyimides," *Journal of Applied Physics*, vol. 86, no. 5, pp. 2473–2478, 1999.

[29] G. Barbero, D. Olivero, N. Scaramuzza, G. Strangi, and C. Versace, "Influence of the bias-voltage on the anchoring energy for nematic liquid crystals," *Physical Review E: Statistical, Nonlinear, and Soft Matter Physics*, vol. 69, no. 2, Article ID 021713, pp. 1–21713, 2004.

[30] L. Jinwei, Z. Suhua, Y. Yuying, A. Hailong, Z. Zhendong, and Y. Guochen, "The influences of surface polarization on NLC cells," *Liquid Crystals*, vol. 34, no. 12, pp. 1425–1431, 2007.

[31] R.-H. Guan, W.-J. Ye, and H.-Y. Xing, "Influences of surface and flexoelectric polarization on the effective anchoring energy in nematic liquid crystal," *Chinese Physics B*, vol. 24, no. 10, Article ID 106102, 2015.

[32] M. Rahimi, T. F. Roberts, J. C. Armas-Pérez et al., "Nanoparticle self-assembly at the interface of liquid crystal droplets," *Proceedings of the National Acadamy of Sciences of the United States of America*, vol. 112, no. 17, pp. 5297–5302, 2015.

[33] O. Lavrentovich, B. Lev, and A. Trokhymchuk, "Liquid crystal colloids," *Condensed Matter Physics*, vol. 13, no. 3, pp. 330021-330022, 2010.

[34] G. Barbero and L. R. Evangelista, *An Elementary Course on the Continuum Theory for Nematic Liquid Crystals*, World Scientific, Singapore, 2001.

[35] W. H. Press, S. A. Teukolsky, W. T. Vetterling, and B. P. Flannery, *Numerical Recipes in Fortran*, Cambridge University Press, 1992.

[36] G. Barbero, F. Simoni, and P. Aiello, "Nonlinear optical reorientation in hybrid aligned nematics," *Journal of Applied Physics*, vol. 55, no. 2, pp. 304–311, 1984.

[37] J. A. Reyes and R. Rodríguez, "Waveguiding in a Nematic Hybrid Slab," *Molecular Crystals and Liquid Crystals*, vol. 317, no. 1, pp. 135–151, 1998.

[38] J. A. Olivares, R. F. Rodríguez, and J. A. Reyes, "Ray tracing and reflectivity measurements in nematic hybrid cells," *Optics Communications*, vol. 221, no. 4-6, pp. 223–239, 2003.